LASER-INDUCED NANOSTRUCTURING

Jörn BONSE[1,*], Eric RAHNER[2], Heike VOSS[1], Klaus SOKOLOWSKI-TINTEN[3], Stephan GRÄF[2]

[1] Bundesanstalt für Materialforschung und -prüfung (BAM), Berlin, Germany

[2] Friedrich Schiller University Jena, Jena, Germany

[3] University of Duisburg-Essen, Duisburg, Germany

*** joern.bonse@bam.de**

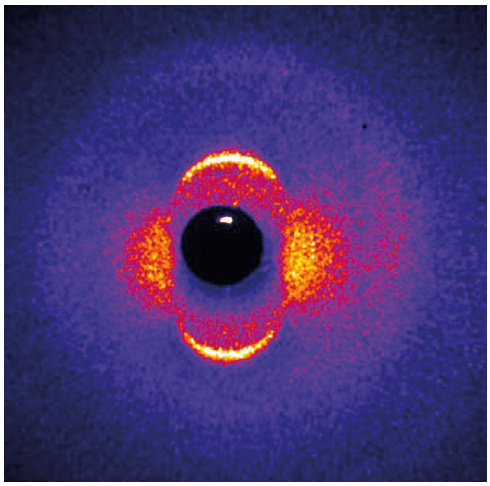

The laser-induced fabrication of nanostructures with feature sizes below the optical diffraction limit is possible for almost any material for arbitrary sample geometries and dimensions by exploiting nonlinear excitations or optical near-field interactions. This overview highlights historical milestones, explains the underlying physical processes and associated challenges, and discusses current and future trends in the field of ultrafast laser nanostructuring.

https://doi.org/10.1051/photon/202613748

Laser-Induced Nanostructuring (LIN) represents one of the thriving industrial demands of the past years [1]. It appears simple and appealing to flexibly functionalize either tiny sample spots or large-area surfaces in a single, contactless, aseptic, and cost-effective processing step that can be even conducted under ambient conditions. This expectation is seeded by the enormous developments in laser technology over the past decades, featuring a Moore-law like scaling through an output power-doubling of *Ultrashort Pulsed Lasers* (UPLs) about every two years. Currently, UPLs emitting in the near-infrared (NIR) or visible spectral range are commercially available at the 10 kW average power level, featuring MHz to GHz pulse repetition rates, while providing µJ to mJ pulse energies. Combined with state-of-the-art scanner technology, this puts areal laser processing rates towards the m^2/s at sight [2].

Unfortunately, the generation of nanoscale structures by simply focussing a laser beam onto a surface or into the volume of a workpiece has to overcome Abbe's fundamental *optical diffraction limit* for far-field applications. This limit defines a minimum achievable focal spot diameter of about half of the radiation wavelength λ. However, ultrashort laser pulses are reaching enormous peak intensities, which helps to enable LIN.

Figure 1 summarizes how UPLs and their interplay with specific physical effects enable LIN with feature sizes below the classical optical diffraction limit. This setting leads to two fundamental approaches. The first is based on *near-field effects*. Optical near-fields typically occur as evanescent fields in the vicinity of interfaces (known from the effect of total reflection). Through their exponential decay, they rapidly vanish on a length scale of typically 10 nm only. Moreover, in the vicinity of sharp topographical features, optical near-fields can exhibit field amplitudes enhanced by several orders of magnitude. Under certain conditions, the enhancement can be further amplified *via* resonant excitation channels, such as *Plasmons*.

The second approach towards LIN is based on *nonlinear absorption*: Several (*m*) photons are simultaneously absorbed from a laser beam

in the sample material, with a transition probability scaling with I^m (I: local intensity). Hence, for a Gaussian laser beam, the profile of nonlinearly excited electrons radially narrows (depending on m) and is confined in the center of the laser beam. Thus, the interaction of high-intensity laser beams with wide bandgap dielectrics can confine the deposited optical energy to the nm-scale.

However, the exploitation of locally confined or enhanced optical absorption for LIN is only successful if the deposited optical energy remains spatially confined until it is transferred to the lattice. This becomes neatly possible for UPLs since their duration is shorter than the typical *electron-phonon relaxation* times that determine how fast a material can be heated. As consequence of this energy confinement during the laser pulse absorption and the subsequent transfer to the lattice, the so-called *heat-affected zone* (HAZ) surrounding the initially irradiated material volume is minimized. For sub-picosecond pulse durations, it extends typically a few tens to hundreds of nanometers into the surrounding.

Finally, UPL-induced damage of irradiated materials is often very deterministic with sharply defined threshold intensities/fluences. If a laser with a Gaussian beam profile is then operated just above the damage threshold, sub-micrometric damage sites can be created in the center of the focussed spot. The need to work very precisely at a peak fluence close to the damage threshold, in turn, imposes rather strict requirements on the pulse-to-pulse stability of the laser. Here, major advances have been made thanks to solid-state laser technologies, which play a key role in the latest generations of UPLs.

In brief, for rendering LIN possible, the ultrashort pulse duration is essential as it translates to high peak intensities and enables energy confinement through nonlinear or near-field effects, along with sharp fluence thresholds for material modifications, and a controlled material response *via* a minimized HAZ.

LASER-INDUCED SURFACE AND VOLUME NANOSTRUCTURING

EXPERIMENTAL IMPLEMENTATIONS OF LIN

Since the turn of the millennium, enormous progress has been made by demonstrating LIN through different experimental implementations. At the same time, significant advances have been achieved in the scientific understanding and control of the physical and chemical effects, as well as in the improvement of engineering aspects. Figure 2 provides a collage highlighting some selected LIN results. The experimental methods can be categorized in surface processing (left panels) and volume processing (right panels). Within each of those methods, LIN can be realized either through direct focussing (top panels) allowing a punctual nanoscale material modification or sculpturing, or it can be realized through matter self-ordering effects (bottom panels). The latter are enabled via coherent optical scattering and matter redistribution in the spatially extended focal regions upon loose focussing often realized along with laser beam scanning.

Joglekar *et al.* [3] demonstrated the concept of combining direct focussing of a NIR fs-laser beam with a high numerical aperture (NA) microscope objective onto the surface with nonlinear absorption effects in a glass sample (Fig. 2(a.I)). With a Gaussian focal spot diameter of $2w_0 = 0.41$ µm they obtained surface crater diameters of a few tens of nanometers only. Belloni *et al.* [4] also used direct focussing but employed a beam-shaping spatial light modulator and interference for creating a doughnut-shaped first-order Bessel beam at the rear-surface of a sapphire crystal. Utilizing a single Ti:sapphire fs-laser pulse, they were able to eject a nano-pillar-like, still crystalline sapphire rod of less than 1 µm in diameter with a length of ≈10 µm (Fig. (2a.II)). Juodkazis *et al.* [5] focussed single Ti:sapphire fs-laser pulses tightly into the volume of the sapphire for generating bulk-confined micro-explosions (Fig. 2(b.I)). Cross-sectional inspection by scanning electron microscopy (SEM) revealed the formation of a tear-drop-shaped nano-void with a diameter of a few hundred nm, surrounded by a sub-µm shell of amorphous material embedded in a locally defective crystal. When reducing the pulse energy and increasing the number of laser pulses applied per tightly focussed laser spot, void-less local material modifications can be generated in the volume of the laser-irradiated material. This can be used, *e.g.*, for writing optical waveguides in glasses, or for 3D additive manufacturing on the nanoscale by using two-photon-polymerization in suitable organic liquids. Cao *et al.* [6] used this sub-ablative NIR fs-laser bulk scan processing strategy at high pulse repetition rates (500 kHz) to locally crystallize a lithium niobate-silicate multi-component glass, visualized in Fig. 2(b.II) in cross-section by SEM and electron backscatter diffraction for different laser processing conditions. Loose focussing with low NA optics also provides the possibility of LIN at the surface and in the volume of solids. At first glance, this appears counterintuitive since ● ● ●

Figure 1. Physical effects and technologies for jointly enabling LIN.

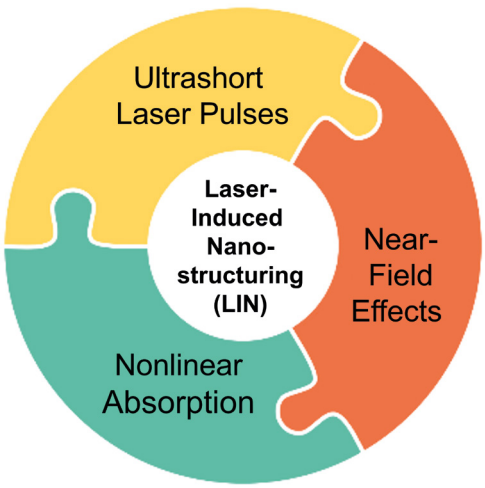

the focussed laser beam spot sizes exceed the desired size of the laser-induced nanostructures by orders of magnitude. However, here intra-pulse coherent scattering and near-field interference effects emerging in the laser-irradiated area/volume can seed periodic nanoscale patterns of the absorbed optical energy. The latter are subsequently transferred to the lattice of the solid and eventually imprinted as a corrugated surface topography or in sub-ablative periodic volume modifications. These two scenarios of LIN are demonstrated in the lower part of Figure 2. The left panel (Fig. 2(c)) collects SEM images of several different types of so-called *Laser-Induced Periodic Surface Structures* (LIPSS). They are classified as *Low Spatial Frequency LIPSS* (LSFL), *Triangular Nano-Pillars* (TNP), or *Hexagonally-Arranged Nanostructures* (HAN) – all with spatial periods close to λ, or as *High Spatial Frequency LIPSS* (HSFL) having periods down to the tens to hundreds of nm range, *i.e.*, far below the optical diffraction limit [1,7]. HSFL are solely formed upon irradiation with UPLs. The right panel (Fig. 2(d)) assembles results from

Figure 2. Selected LIN results and their methodic categorization into surface and volume processing (columns), while using direct focussing or selfordering effects (rows). Figure 2(a)I (bottom) reprinted from [3] Copyright (2004) National Academy of Sciences, U.S.A.; Figure 2(a)II (top and bottom right) reprinted from [4] Copyright 2023 under Creative Commons BY-NC-ND 4.0 license, and with permission from the authors of that article (F. Courvoisier.); Figure 2(b)I (bottom) reprinted with permission from [S. Juodkazis *et al.*, Phys. Rev. Lett., 96, 166101, 2006] Copyright (2006) by the American Physical Society.; Figure 2(b) II reprinted with permission from [6]. Copyright 2019 American Chemical Society; Figure 2(c)I reprinted from [S.V. Kirner, *et al.*, J. Appl. Phys. **122**, 104901 (2017), with the permission of AIP Publishing; Figure 2(c)II (top) reprinted from [S. van der Poel, *et al.*, Lubricants 7, 70 (2019)] Copyright 2019 under Creative Commons BY 4.0 license; Figure 2(c)II (bottom) adapted from [L. Porta-Velilla, *et al.*, Nanomaterials **12**, 2380 (2022)] Copyright 2022 under Creative Commons BY 4.0 license; Figure 2(d)I reprinted with permission from [8]. Copyright 2017 American Chemical Society; Figure 2(d)II used with permission of Royal Society of Chemistry from [Mater. Horiz., N. Sharma *et al.*, 6, 978-983, 2019]; permission conveyed through Copyright Clearance Center, Inc.

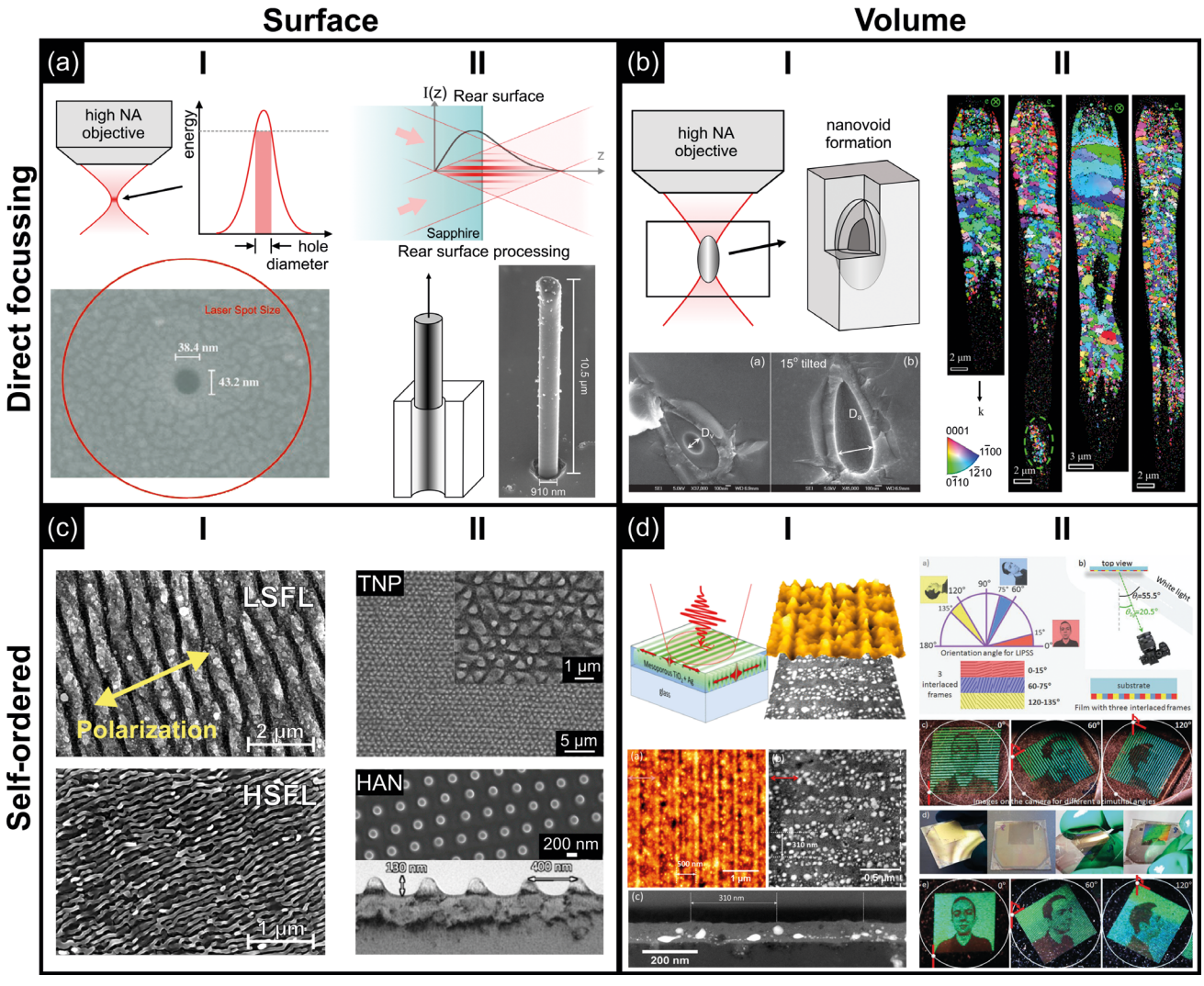

fs-laser processed metal-ion doped titania films that were subjected to scan-processing [8]. Here, the coherent scattering and interference leads to a 3D spatially patterned deposition of the laser pulse energy that, in turn, promotes the local precipitation and formation of plasmonic metallic nanoparticles (NP), see Fig. 2(d.I). These NP, being periodically spaced and arranged in different layers, allow the generation of macroscopically visible structural color effects and can serve to encode view-point dependent images as security tags (Fig. 2(d.II)) [9].

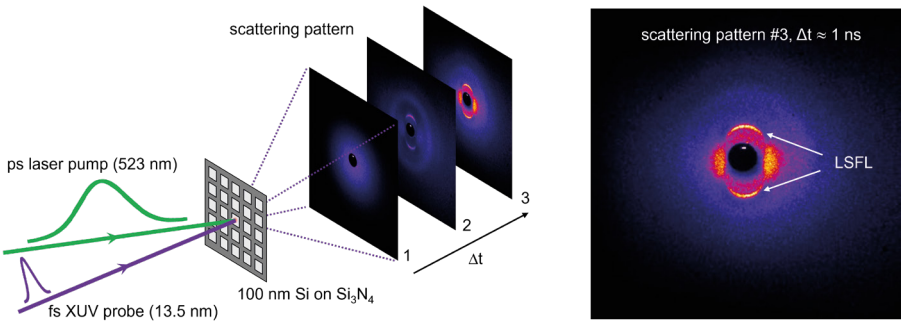

Figure 3. Time-resolved scattering experiment performed at the FEL FLASH in Hamburg [1,10]. The scattering patterns are recorded by a CCD camera that is synchronized with the fs-XUV probe pulses. (Adapted from [10], © 2024 under Creative Commons BY 4.0 license. Retrieved from https://doi.org/10.1002/lpor.202300912).

ADVANCED CHARACTERISATION OF NANOSTRUCTURES

A problem that immediately emerges with the successful realization of LIN is that conventional optical far-field characterization methods – such as optical microscopy – are no longer applicable for *in-situ* evaluation of the LIN results. Hence, either slow scanning probe or near-field optical characterization techniques, or far-field spectral ensemble measurements are required. The latter refer, *e.g.*, to optical scattering from NP, where the scattered light is spectrally resolved and analysed in the far-field. Alternatively, shorter wavelength electromagnetic radiation may be applied, pushing the required photon energies into the XUV- or X-ray spectral range.

In this direction, the development of short wavelength *Free Electron Lasers* (XFELs) has opened up exciting new possibilities since these sources combine an extremely high tuneable photon flux with spatial coherence and pulse durations in the fs- or even as-range. The potential of such short wavelength and ultrashort-pulsed radiation sources for studying the multi-scale processes transiently manifesting in laser processing was recently reviewed in [10]. XFELs allow, for example, the *in-situ* investigation of laser-driven structure formation at extreme scales in space and time *via* fs-pump-probe *small-angle X-ray scattering* (fs-SAXS) or even *grazing-incidence small-angle X-ray scattering* (fs-GISAXS). This covers the entire spatial range from atomic scales, over the nano- and meso- towards the micro-scale, while simultaneously covering temporal observation ranges up to ms, probed with sub-ps temporal resolution. Apart from clarifying the dynamics of ultrafast phase transitions or the formation mechanisms of the HSFL [7] featuring ≈100 nm spatial period only, also the disintegration of a laser-molten surface layer into voids and NP during fs laser ablation can be successfully revealed [11].

Figure 3 exemplifies a time-resolved single-pulse scattering pump-probe experiment (ps optical pump with $\lambda = 523$ nm / fs XUV probe with $\lambda = 13.5$ nm) performed in transmission geometry on a 100 nm thin silicon film at the FLASH FEL at DESY (Hamburg, Germany) [1,10]. A sequence of pump-probe far-field scattering patterns acquired at different delay times Δt allow to record in a stroboscopic fashion the spatial frequency distributions of the laser-induced nanostructures. For example, the characteristic double-arc feature arranged symmetrically in the vertical direction on pattern #3 ($\Delta t \approx 1$ ns) represents the transient signature of classical LSFL ("wavelength ripples") formed on laser-molten silicon and featuring spatial periods of ≈ 300 nm, here.

PROCESSING OF LIPSS AND THE CONTROL OF REGULARITY

In the following, we will focus on LIPSS as an example of LIN with a tremendous technological and industrial potential, having surface functionalization applications in the fields of optics, tribology, and medicine. Figure 4 visualizes LSFL and HSFL created on the surface of titanium by LIN in a laser beam scanning approach with an industrial laser system (1030 nm, 860fs, 10 kHz). For both types of LIPSS, the left panel shows an SEM image with the same magnification, while the right panel displays a two-dimensional *Fast Fourier Transform*, representing the spatial frequency distributions of the corresponding spatial domain. LSFL are formed perpendicular to the linear laser beam polarisation indicated by the double-arrows, while the HSFL are rotated by 90°.

The LSFL have a most frequent period of $\hat{\Lambda} = 773$ nm, with standard deviation of $\Delta\hat{\Lambda} = \pm 44$ nm. For the much smaller HSFL, values of $\hat{\Lambda} \pm \Delta\hat{\Lambda} = (87 \pm 12)$ nm can be deduced, *i.e.*, $< \lambda/10$. Comparing the 2D-FFTs of both types of LIPSS, it becomes clear that their signatures differ remarkably: While the LSFL are represented by a pair of sickle-shaped, radially asymmetric arcs, the HSFL appear as a pair of broad, radially symmetric "clouds". The ratio of the spread of the periods to the most frequent spatial • • •

period value reveals that the LSFL have better regularity (smaller ratio $R = \Delta\hat{\Lambda}/\hat{\Lambda}$) than the HSFL. Generally, the regularity of LIPSS is better, as sharper their peaks in the Fourier domain are, *i.e.* as smaller *R*.

The technological potential of LIPSS for functional surface engineering critically depends on how regular and homogeneous these self-organized patterns are. Although many studies have shown how laser parameters, material properties, and optical effects influence LIPSS formation, assessing the quality of the resulting structures has remained a major challenge. The main reason is that suitable routines and software programs for automated evaluation were not available. Instead, evaluations were often performed purely visually or based on partly automated Fourier-based methods. Thus, the subjective influence of the person performing the analysis is a central problem, as the evaluation criteria are defined manually and the complex surface morphologies are usually reduced to a single indicator. This significantly limits the comparability between assessments and slows down systematic process optimisation.

With the introduction of *ReguΛarity* [12], a free, fully automated software tool developed specifically to quantify the regularity of LIPSS from microscope images, the transition from subjective, case-specific assessments to a standardised and reproducible description of LIPSS quality has been achieved. Instead of relying on a single metric, several complementary descriptors form a multi-parameter regularity tuple that is used to evaluate LIPSS. This approach considers that LIPSS regularity is multifaceted: highly functional surfaces require not only a precisely defined average period, but also low local period fluctuations, uniform alignment, spatial homogeneity and continuous phase development.

By enabling fast, objective and high-throughput regularity analysis, new perspectives are opening up for LIPSS research and applications. *ReguΛarity* supports the data-driven optimisation of laser processes, facilitates comparisons between different materials and laboratories, and lays the foundation for machine learning-assisted design of functional laser-structured surfaces. In this sense, the software represents an important step in transforming LIPSS from a complex physical phenomenon into a reliably machinable surface technology.

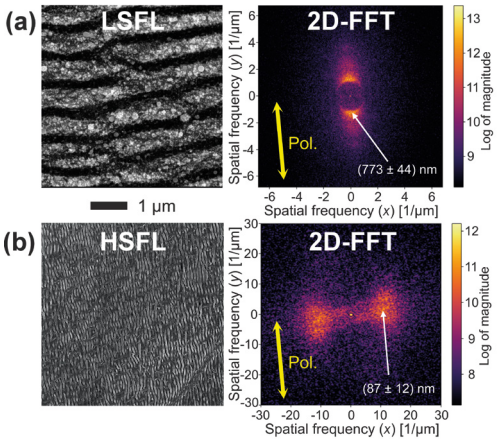

Figure 4. LIN of two types of LIPSS (LSFL and HSFL) on titanium featuring different spatial periods, orientations, and regularities. SEM images (left) and two-dimensional Fast Fourier Transforms (2D-FFT, right). The double-arrows indicate the direction of the linear laser beam polarisation.

CURRENT AND FUTURE TRENDS

Currently, several trends are emerging in the field of LIN. One direction concerns the transfer of specific surface functionalities demonstrated in the laboratory into robust industrial and everyday applications. This includes the development of antibacterial surfaces in medical or public settings, or the development of bioactive surfaces that can improve the differentiation or enhanced/reduced growth of certain cells on medical implants. Beyond, nanostructures allow precise control over reflection, transmission, and structural coloration. Such capabilities are relevant for advanced display technologies, improved photovoltaic devices, and high-density optical data storage. The intrinsic irregularity of LIPSS, arising from self-organization processes, further enables the fabrication of non-cloneable security features for product authentication. In tribological systems, LIN can reduce friction and wear under sliding contact, lowering energy consumption and extending the operational lifetime of mechanical components.

A second trend focusses on deepening the fundamental understanding of the underlying processes. Ultrafast laser-matter interactions involve highly non-equilibrium dynamics starting already on fs to ps timescales, where nonlinear optical effects, transient electronic excitation, and rapid phase transitions interplay. Time-resolved experimental techniques are, therefore, increasingly employed to resolve ultrafast carrier dynamics, energy transfer pathways, and the onset of structure formation. In parallel, multi-scale modeling approaches are advancing, combining electrodynamics with molecular dynamics, hydrodynamic and thermomechanical descriptions to capture the coupled evolution of electromagnetic fields, electron-phonon interactions, structural changes, melt flows, pressure waves, and resolidification.

A third trend addresses scaling and manufacturing strategies required for industrial implementation [2]. Modern UPLs operating at repetition rates of several hundred kHz to several MHz along with fast beam deflection systems, such as high-speed polygon scanners, in combination with adaptive optical elements, enable large-area processing at high throughput. Optical parallelization concepts – employing diffractive optical elements or spatial light modulators – allow the simultaneous generation of multiple structured spots, significantly enhancing productivity. Automated quality assurance through *in-situ* monitoring and feedback control is becoming increasingly important to ensure process stability and reproducibility

under industrial conditions. In this context, the integration of artificial intelligence and machine learning represents a transformative development. Data-driven predictive modeling can link process parameters to resulting nanostructures and their functionalities, enabling accelerated optimization, adaptive process control, and the identification of previously unexplored parameter regimes. At the same time, such predictive approaches can save energy and material resources, further developing laser processing towards a green laser technology. Overall, scaling of LIN is less about overcoming a single physical limit than about intelligently combining self-organization, optical parallelization, fast beam delivery, and advanced laser sources.

CONCLUSION

This review presented a brief summary of important milestones in the field of LIN of solids with surface- or volume-related features sizes below the diffraction limit. Features smaller than one-tenth of the laser wavelength can be realized. This is made possible by the minimal HAZ achieved by the ultrashort pulse durations and high intensities, which effectively drive nonlinear excitation processes and enable coherently excited collective near-field optical effects. Such tiny structures then require advanced characterization techniques as they are provided through XFELs, to investigate even *in-situ* the formation mechanisms at extreme scales in space (nm to µm) and time (fs to ms). A special focus was on LIPSS that are often manifesting in laser processing. Recent developments and trends in their generation, characterisation, and scaling were outlined, and the potential for further promoting their use in industrial applications was highlighted.

ACKNOWLEDGEMENTS

This work was funded by the Deutsche Forschungsgemeinschaft (DFG, German Research Foundation) through Project IDs 530345255 and 278162697-SFB 1242.

REFERENCES

[1] R. Stoian and J. Bonse (eds.), Ultrafast Laser Nanostructuring — The Pursuit of Extreme Scales (Springer, Cham, 2023)

[2] J. Bonse and A.F. Lasagni (eds.), Scaling of Laser Processing — Making Light Matter (Springer, Cham, 2026)

[3] A.P. Joglekar, H. Liu, E. Meyhöfer *et al.* Proc. Natl. Acad. Sci. U.S.A. **101**, 5856 (2004)

[4] V.V. Belloni, M. Hassan, L. Furfaro *et al.* Laser Photon. Rev. **18**, 2300687 (2024)

[5] S. Juodkazis, K. Nishimura, S. Tanaka *et al.* Phys. Rev. Lett. **96**, 166101 (2006)

[6] J. Cao, M. Lancry, F. Brisset *et al.* Crystal Growth & Design **19**, 2189 (2019)

[7] J. Bonse and S. Gräf, Laser Photon. Rev. **14**, 2000215 (2020)

[8] Z. Liu, J. Siegel, M. Garcia-Lechuga *et al.* ACS Nano **11**, 5031 (2017)

[9] N. Sharma, M. Vangheluwe, F. Vocanson *et al.* Mater. Horiz. **6**, 978 (2019)

[10] J. Bonse and K. Sokolowski-Tinten, Laser Photon. Rev. **18**, 2300912 (2024)

[11] Y. Sun, C. Chen, T.J. Albert *et al.*, Commun. Mater. **6**, 69 (2025)

[12] E. Rahner, T. Thiele, H. Voss *et al.* Appl. Surf. Sci. **726**, 165919 (2026)